24th COBEM - 2017

24th ABCM International Congress of Mechanical Engineering
December 3-8, 2017, Curitiba, PR, Brazil

COBEM-2017-1887
ANALYSIS OF A FLEXIBLE ROTATING SHAFT SUPPORTED BY HYDRODYNAMIC BEARINGS CONSIDERING UNCERTAINTIES

Layane R. S. Queiroz
Romes A. Borges
Institute of Mathematics and Technology, Federal University of Goiás – Campus Catalão, Catalão-GO, Brazil.
spinellyh@gmail.com, romes@ufg.br.

Aldermir A. Cavalini Jr.
Valder Steffen Jr.
School of Mechanical Engineering, Federal University of Uberlândia, Uberlândia-MG, Brazil.
aacjunior@mecanica.ufu.br, vsteffen@mecanica.ufu.br.

Abstract. *This paper considers the application of the Latin Hypercube sampling and the homogeneous Polynomial Chaos expansion aiming at considering uncertainties of a flexible rotor. The system contains two rigid discs and a horizontal shaft, which is supported by two cylindrical hydrodynamic bearings. The shaft is flexible and represented by a finite element model based on the Timoshenko beam theory. The hydrodynamic supporting forces are determined from the solution of the so-called Reynolds equation. Although hydrodynamic bearings can offer a long operation life, variations in the radial clearance and oil film temperature can affect the dynamic behavior of the system. In this context, this work is devoted to the analysis of uncertainties in the bearings radial clearance and oil film temperature affecting the dynamic behavior of the rotating machine. Computational tests showed that the Latin Hypercube and the Polynomial Chaos are able to approximate the deterministic solution precisely, where the Polynomial Chaos is indeed more accurate.*

Keywords: *flexible rotor, hydrodynamic bearing, polynomial chaos, Latin hypercube sampling.*

1. INTRODUCTION

Rotating machines are mechanical systems commonly found in different industrial equipment, with applications in automotive, aerospace, aviation, energy, and petroleum. According to Muszynska (2005), a rotating machine is composed by shafts, discs, impellers, couplings, gears, bearings, among others.

In this work, we consider a flexible steel shaft with two rigid discs and supported by two cylindrical hydrodynamic bearings. This rotor configuration was studied by Cavalini Jr *et al*. (2015), considering uncertainties in components of the bearings, using a fuzzy logic approach. Machado e Cavalca (2015) proposed a numerical model to analyze the wear in the wall of hydrodynamic bearings for a study in the frequency domain. Cai e Xiao (2016) studied the nonlinear instability phenomena in a shaft with rolling bearings that is caused by the contact and friction between the shaft and the stationary mechanism of the rotating machine. Mendes *et al*. (2017) investigated the influence of wear depth and angular position associated with the hydrodynamic bearing wear parameters.

The rotor under consideration has its equation of motion determined by applying the finite element method and the Lagrange's equation. In the present work, it is assumed that there are uncertainties in the shaft diameter specifically at the position of the bearings, representing the variability that may occur in the radial clearance, and in the oil film temperature of the bearings. It is important to mention that the operating conditions of rotating machines affect the oil temperature and, then, it may change its lubrication characteristics. In the same way, the distance between the shaft and the bearing may eventually change due to the wear or even due to tolerances related to the machining of parts.

For the quantification of the uncertainties, the Polynomial Chaos (PC) expansion is used. The obtained results are compared with those from the Latin Hypercube sampling and the deterministic solution. The Latin Hypercube exhibits a convergence rate better than the Monte Carlo method, since it requires a small number of samples as compared with the Monte Carlo (Viana, 2016). PC considers a basis of orthogonal polynomials in which the weight function is in accordance with the probability density function of the random variables that are used to handle the uncertainties. Therefore, it is possible to separate, in the obtained solution, the stochastic part, which is concentrated in the basis of polynomials used (Ghanem and Spanos, 1991).

Ghanem e Spanos (1991) presented a detailed description of the Karhunen-Loève expansion, focusing on how to obtain the PC with the Hermite orthogonal polynomials. Xiu e Karniadakis (2002) generalized the PC for the families of orthogonal polynomials listed in the Askey-scheme, such that the random variables can be associated to other probabilistic distributions. In Sinou e Jacquelin (2015), a shaft with uncertainties in the stiffness and in the symmetrical coupling terms that are time-dependent was analyzed in its critical speeds by applying the stochastic harmonic balance method and PC. Daróczy *et al*. (2016) worked on the project of H-Darrieus wind turbines by considering the PC to deal with uncertainties in the vibration control angle and the angular velocity.

2. POLYNOMIAL CHAOS

The PC expansion was defined over the Hermite orthogonal polynomials for second order stochastic processes (i.e., processes for which the variance is finite), considering independent Gaussian random variables in the Hilbert space L^2 (Xiu *et al*., 2003).

According to Ghanem e Spanos (1991), the system's random solution is a stochastic second order process $X(w)$ in which w represents a random event. This process can be denoted as a PC expansion, which is:

$$X(w) = \sum_{j=0}^{\infty} \hat{a}_j \Phi_j(\boldsymbol{\xi}) \tag{1}$$

where $\hat{a}_j$ is the j-th expansion's coefficient; $\Phi_j(\boldsymbol{\xi})$ is the polynomial chaos of order p and dimension $n = \infty$, which is orthogonal in terms of the Gaussian random variables in $\boldsymbol{\xi} = \left(\xi_{i_1}, \xi_{i_2} \ \ldots, \xi_{i_n}\right)$.

The polynomials in $\boldsymbol{\Phi} = \{\Phi_1, \Phi_2, \ldots\}$ create a complete orthogonal basis in terms of the independent random variables $\boldsymbol{\xi}$, such that the inner product coincides with the expected value E in the Hilbert space (Lucor *et al*., 2004), that is:

$$\langle \Phi_r, \Phi_s \rangle = E[\Phi_r, \Phi_s] = \int_C \ \Phi_r(\boldsymbol{\xi}) \Phi_s(\boldsymbol{\xi}) \rho(\boldsymbol{\xi}) d\boldsymbol{\xi} \tag{2}$$

where $\rho(\boldsymbol{\xi})$ is the weight function and C is the support (orthogonality interval). The weight function must agree with the probability distribution function of the random variables $\boldsymbol{\xi}$ under consideration. For the homogeneous PC, C represents the interval $(-\infty, \infty)$ and the weight function of the Hermite orthogonal polynomials is the probability density function associated to the n-dimensional Gaussian random variables.

In the homogeneous PC expansion, the polynomial chaos $\Phi_j(\boldsymbol{\xi})$, with order p and dimension n, corresponds to the Hermite n-dimensional polynomial (Ghanem and Spanos, 1991):

$$\Phi_j(\boldsymbol{\xi}) = (-1)^n \left(e^{\frac{1}{2}\boldsymbol{\xi}^T\boldsymbol{\xi}}\right) \left(\frac{\partial^n}{\partial\xi_1 \partial\xi_2 \ldots \partial\xi_n} e^{-\frac{1}{2}\boldsymbol{\xi}^T\boldsymbol{\xi}}\right) \tag{3}$$

The coefficients in Eq. (1) are obtained by projecting the random solution over each polynomial of the basis $\boldsymbol{\Phi}$, considering the inner product, that is:

$$\hat{a}_j = \frac{\langle X(\xi), \Phi_j(\xi) \rangle}{\langle \sum_{i=0}^{\infty} \Phi_i(\xi), \Phi_j(\xi) \rangle} = \frac{\int_C \ X(\xi) \Phi_j(\xi) \rho(\xi) d\xi}{\langle \ \Phi_j(\xi), \Phi_j(\xi) \rangle} \tag{4}$$

The statistics of the random solution $X(w)$, in particular, its mean and variance are expressed by, respectively:

$$\mu_X = \hat{a}_0 \tag{5}$$

$$\sigma_X^2 = \sum_{j=1}^{\infty} \hat{a}_j^2 \langle \Phi_j^2 \rangle \tag{6}$$

Equation (1) has an infinite expansion that needs to be changed to a finite one, which similarly suggest to consider a finite number of random variables. Tables with polynomial chaos of fourth order ($p = 4$) and with up to four dimensions ($n = 4$ random variables), considering the Hermite polynomials in the basis, can be found in Ghanem e Spanos (1991).

3. ROTOR MODELING

The flexible shaft is represented by Timoshenko beams and has two rigid discs, besides being supported by two cylindrical hydrodynamic bearings. It is also considered an unbalanced force, which is a mass acting near to the shaft's geometrical center, and supporting forces related to the bearings action. The cylindrical hydrodynamic bearings have a lubricant fluid film that avoids direct contact between the shaft and the bearings (i.e., there is no contact between the metal components) and work in accordance with the theory of hydrodynamic lubricant.

The dynamic behavior of the studied rotor is modeled by applying the following steps (Lalanne and Ferraris, 1998): obtain the kinetic energy T and the strain energy U of the components composing the rotor, besides obtaining the virtual work of the external forces; apply the finite element method; and, apply the Lagrange equations for the independent generalized coordinates and the generalized forces acting on the rotor. Then, these steps are combined together and allow to obtain the matrices related to the general equation of motion.

It follows that the differential equation of motion of the flexible rotor with hydrodynamic bearings is given as presented in Cavalini Jr *et al*. (2015):

$$\boldsymbol{M}\ddot{\boldsymbol{q}} + \left[\boldsymbol{D} + \Omega \boldsymbol{D}_g\right]\dot{\boldsymbol{q}} + \left[\boldsymbol{K} + \dot{\Omega}\boldsymbol{K}_{st}\right]\boldsymbol{q} = \boldsymbol{W} + \boldsymbol{F}_u + \boldsymbol{F}_h \tag{7}$$

where $\boldsymbol{M}$, $\boldsymbol{D}$, $\boldsymbol{D}_g$, $\boldsymbol{K}$, $\boldsymbol{K}_{st}$, $\boldsymbol{W}$, $\boldsymbol{F}_u$, and $\boldsymbol{F}_h$ are, respectively, the global matrices of mass, proportional damping, gyroscope effect, stiffness, stiffness from the transient motion, weight of the rotating parts, unbalance forces, and hydrodynamic supporting forces. The damping matrix is given by $\boldsymbol{D} = \lambda\boldsymbol{M} + \beta\boldsymbol{K}$, with constants λ and β. The shaft rotation speed and acceleration is given by Ω and $\dot{\Omega}$, respectively. The vectors of generalized displacements, velocities, and accelerations are, respectively, $\boldsymbol{q}$, $\dot{\boldsymbol{q}}$, and $\ddot{\boldsymbol{q}}$.

The finite element model of the flexible rotor is illustrated in Fig. 1, in which there are 17 nodes and 16 Timoshenko beam elements. The two discs and the two bearings are coupled in the model nodes. Moreover, each node has four degree of freedom, two ones associated with the displacements and the others with rotations.

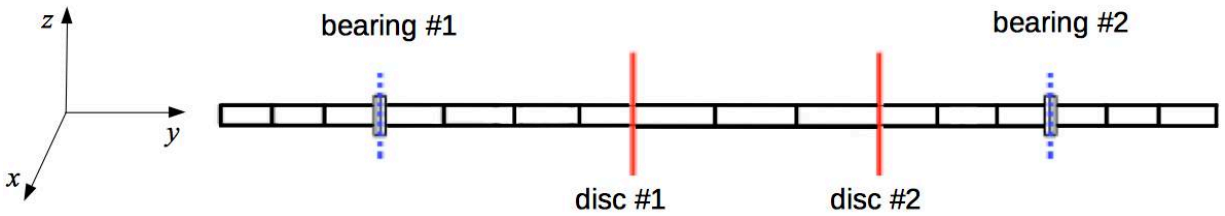

Figure 1. Finite element model of the flexible rotor with its components.

The cylindrical hydrodynamic bearings are treated as support elements and they are assumed as short journal bearings (i.e., the ratio between the width and diameter is less than 0.5). The mathematical modeling of the supporting forces considers the non linear model proposed by Capone (1986), which solves the Reynolds' equation in (7) for isothermal and laminar flow.

$$\left(\frac{R}{L_h}\right)^2 \frac{\partial}{\partial \bar{y}}\left(\bar{h}_h^3 \frac{\partial \bar{p}_h(\theta,\bar{y})}{\partial \bar{y}}\right) = \frac{\partial \bar{h}_h}{\partial \theta} + 2\dot{\bar{h}}_h \tag{8}$$

where $\bar{p}_h(\theta,\bar{y})$ is the pressure distribution on the bearing; $\bar{x}$, $\bar{y}$, and $\bar{z}$ are the dimensionless coordinates of the shaft's center for the respective directions x, y, and z in which $\bar{x} = \frac{x}{C}$, $\bar{z} = \frac{z}{C}$, $\dot{\bar{x}} = \frac{\dot{x}}{\omega C}$, and $\dot{\bar{z}} = \frac{\dot{z}}{\omega C}$; C is the radial clearance; ω is the shaft's rotation speed; θ is the cylindrical coordinate; L_h is the bearing's length; R is the shaft's radius; $\bar{h}_h$ is the dimensionless oil film thickness, with $\bar{h}_h = \bar{x}\cos\theta - \bar{z}\sin\theta$.

Cavalini Jr *et al*. (2015) made some simplifications in Eq. (8) in order to obtain the analytical expression of the pressure field, resulting in:

$$\bar{p}_h(\theta,\bar{y}) = \frac{1}{8}\left(\frac{L_h}{R}\right)^2 \left[\frac{(\bar{x}-2\dot{\bar{z}})\sin\theta - (\bar{z}+2\dot{\bar{x}})\cos\theta}{\bar{h}_h^3}\right](4\bar{y}^2 - 1) \tag{9}$$

Therefore, the hydrodynamic force $\boldsymbol{F}_h$ considers Eq. (9) being integrated over the bearing area in the variables θ and $\bar{y}$, that is:

$$\boldsymbol{F}_h = -\frac{6\mu\omega R^3}{L_h}\int_{-\frac{1}{2}}^{\frac{1}{2}}\int_{\alpha_h}^{\alpha_h+\pi} \bar{p}_h(\theta,\bar{y})\begin{bmatrix}\cos\theta \\ \sin\theta\end{bmatrix} d\theta d\bar{y} \tag{10}$$

where μ is the oil viscosity and α_h is the attitude angle defined as:

$$\alpha_h = \tan^{-1}\left(\frac{\bar{z}+2\dot{\bar{x}}}{\bar{x}-2\dot{\bar{z}}}\right) - \frac{\pi}{2}\,\mathrm{sign}\left(\frac{\bar{z}+2\dot{\bar{x}}}{\bar{x}-2\dot{\bar{z}}}\right) - \frac{\pi}{2}\,\mathrm{sign}\,(\bar{z}+2\dot{\bar{x}}) \tag{11}$$

4. UNCERTAINTIES IN THE ROTOR

The study considers uncertainties in the cylindrical hydrodynamic bearings parameters. It is assumed that the oil viscosity μ is an uncertain parameter. Moreover, it is considered that the distance between the shaft and the internal part of the bearing, called radial clearance, is an uncertain parameter as well. For the radial clearance, as the parameter C is part of trigonometric and sign functions in Eq. (11), which implies in some numerical difficulties and very slow convergence due to the computation of the integrals that emerge after projecting the space of variables over the polynomial basis for the PC expansion. Then, the strategy that is adopted for the radial clearance considers uncertainties happening to the sections of the shaft's radius R that interact directly with the two bearings.

The application of the homogeneous PC considers that the uncertainties in the oil viscosity are quantified in Eq. (12), for the Gaussian random variable ξ_1, the mean value $\bar{\mu}$, which corresponds to the real value of μ, and the standard deviation $g_1 = \sigma_\mu$ related to the mean value.

$$\tilde{\mu} = \bar{\mu} + \sum_{n=1}^{1} \xi_i g_i = \mu + \xi_1 \sigma_\mu \tag{12}$$

Similarly, it is quantified in Eq. (13) the uncertainties in the radius R, considering the Guassian random variable ξ_2, which is independent of ξ_1, the mean value $\bar{R}$, which corresponds to the real value of R, and the standard deviation $g_2 = \sigma_R$.

$$\tilde{R} = \bar{R} + \sum_{n=2}^{2} \xi_i g_i = R + \xi_2 \sigma_R \tag{13}$$

The uncertainties are propagated in the rotor by considering that the general solution of the motion equation in (7) is represented by a finite homogeneous PC expansion in Eq. (1), for $n = 2$ random variables and a polynomial chaos of maximum order $p = 2$. As the rotor is discretized in finite elements and, then, it is composed of nodes, it follows that the general solution $\boldsymbol{q}(t, \boldsymbol{\xi})$ has the solution for all the degrees of freedom. Therefore, for each node i, which has four degrees of freedom, there is:

$$\begin{bmatrix} \sum_{j=0}^{5} u_{i,j}(t)\Phi_j(\xi_1,\xi_2) \\ \sum_{j=0}^{5} w_{i,j}(t)\Phi_j(\xi_1,\xi_2) \\ \sum_{j=0}^{5} \theta_{i,j}(t)\Phi_j(\xi_1,\xi_2) \\ \sum_{j=0}^{5} \varphi_{i,j}(t)\Phi_j(\xi_1,\xi_2) \end{bmatrix} = \begin{bmatrix} u_{i,0}\Phi_0 + u_{i,1}\Phi_1 + u_{i,2}\Phi_2 + u_{i,3}\Phi_4 + u_{i,4}\Phi_4 + u_{i,5}\Phi_5 \\ w_{i,0}\Phi_0 + w_{i,1}\Phi_1 + w_{i,2}\Phi_2 + w_{i,3}\Phi_3 + w_{i,4}\Phi_4 + w_{i,5}\Phi_5 \\ \theta_{i,0}\Phi_0 + \theta_{i,1}\Phi_1 + \theta_{i,2}\Phi_2 + \theta_{i,3}\Phi_3 + \theta_{i,4}\Phi_4 + \theta_{i,5}\Phi_5 \\ \varphi_{i,0}\Phi_0 + \varphi_{i,1}\Phi_1 + \varphi_{i,2}\Phi_2 + \varphi_{i,3}\Phi_3 + \varphi_{i,4}\Phi_4 + \varphi_{i,5}\Phi_5 \end{bmatrix} \tag{14}$$

After substituting the uncertain parameters, Eqs. (12) and (13), and the solution with the uncertainties propagated, Eq. (14), in the rotor's equation of motion, Eq. (1), it is obtained:

$$\boldsymbol{M}\sum_{j=0}^{5} \ddot{\boldsymbol{q}}_j\Phi_j + \left[\boldsymbol{D} + \Omega\boldsymbol{D}_g\right]\sum_{j=0}^{5} \dot{\boldsymbol{q}}_j\Phi_j + \left[\boldsymbol{K} + \dot{\Omega}\boldsymbol{K}_{st}\right]\sum_{j=0}^{5} \boldsymbol{q}_j\Phi_j = \boldsymbol{W} + \boldsymbol{F_u} + \widetilde{\boldsymbol{F}}_{\boldsymbol{h}} \tag{15}$$

where $\widetilde{\boldsymbol{F}}_{\boldsymbol{h}}$ considers that μ and R are, respectively, substituted by $\tilde{\mu}$ and $\tilde{R}$.

Therefore, after projecting Eq. (15) over the random space for the Hermite orthogonal polynomials basis, it is obtained a set with six equations of motion for the rotor:

$$\begin{cases} \boldsymbol{M}\ddot{\boldsymbol{q}}_0\langle\Phi_0^2\rangle + \left[\boldsymbol{D} + \Omega\boldsymbol{D}_g\right]\dot{\boldsymbol{q}}_0\langle\Phi_0^2\rangle + \left[\boldsymbol{K} + \dot{\Omega}\boldsymbol{K}_{st}\right]\boldsymbol{q}_0\langle\Phi_0^2\rangle = \boldsymbol{W}\langle\Phi_0\rangle + \boldsymbol{F_u}\langle\Phi_0\rangle + \langle\widetilde{\boldsymbol{F}}_{\boldsymbol{h}}, \Phi_0\rangle \\ \boldsymbol{M}\ddot{\boldsymbol{q}}_1\langle\Phi_1^2\rangle + \left[\boldsymbol{D} + \Omega\boldsymbol{D}_g\right]\dot{\boldsymbol{q}}_1\langle\Phi_1^2\rangle + \left[\boldsymbol{K} + \dot{\Omega}\boldsymbol{K}_{st}\right]\boldsymbol{q}_1\langle\Phi_1^2\rangle = \boldsymbol{W}\langle\Phi_1\rangle + \boldsymbol{F_u}\langle\Phi_1\rangle + \langle\widetilde{\boldsymbol{F}}_{\boldsymbol{h}}, \Phi_1\rangle \\ \boldsymbol{M}\ddot{\boldsymbol{q}}_2\langle\Phi_2^2\rangle + \left[\boldsymbol{D} + \Omega\boldsymbol{D}_g\right]\dot{\boldsymbol{q}}_2\langle\Phi_2^2\rangle + \left[\boldsymbol{K} + \dot{\Omega}\boldsymbol{K}_{st}\right]\boldsymbol{q}_2\langle\Phi_2^2\rangle = \boldsymbol{W}\langle\Phi_2\rangle + \boldsymbol{F_u}\langle\Phi_2\rangle + \langle\widetilde{\boldsymbol{F}}_{\boldsymbol{h}}, \Phi_2\rangle \\ \boldsymbol{M}\ddot{\boldsymbol{q}}_3\langle\Phi_3^2\rangle + \left[\boldsymbol{D} + \Omega\boldsymbol{D}_g\right]\dot{\boldsymbol{q}}_3\langle\Phi_3^2\rangle + \left[\boldsymbol{K} + \dot{\Omega}\boldsymbol{K}_{st}\right]\boldsymbol{q}_3\langle\Phi_3^2\rangle = \boldsymbol{W}\langle\Phi_3\rangle + \boldsymbol{F_u}\langle\Phi_3\rangle + \langle\widetilde{\boldsymbol{F}}_{\boldsymbol{h}}, \Phi_3\rangle \\ \boldsymbol{M}\ddot{\boldsymbol{q}}_4\langle\Phi_4^2\rangle + \left[\boldsymbol{D} + \Omega\boldsymbol{D}_g\right]\dot{\boldsymbol{q}}_4\langle\Phi_4^2\rangle + \left[\boldsymbol{K} + \dot{\Omega}\boldsymbol{K}_{st}\right]\boldsymbol{q}_4\langle\Phi_4^2\rangle = \boldsymbol{W}\langle\Phi_4\rangle + \boldsymbol{F_u}\langle\Phi_4\rangle + \langle\widetilde{\boldsymbol{F}}_{\boldsymbol{h}}, \Phi_4\rangle \\ \boldsymbol{M}\ddot{\boldsymbol{q}}_5\langle\Phi_5^2\rangle + \left[\boldsymbol{D} + \Omega\boldsymbol{D}_g\right]\dot{\boldsymbol{q}}_5\langle\Phi_5^2\rangle + \left[\boldsymbol{K} + \dot{\Omega}\boldsymbol{K}_{st}\right]\boldsymbol{q}_5\langle\Phi_5^2\rangle = \boldsymbol{W}\langle\Phi_5\rangle + \boldsymbol{F_u}\langle\Phi_5\rangle + \langle\widetilde{\boldsymbol{F}}_{\boldsymbol{h}}, \Phi_5\rangle \end{cases} \tag{16}$$

The system in Eq. (16) can be solved by a numerical method in order to estimate the statistical answers, which are expressed in terms of the mean and the variance in Eq. (17). Since the equations related to the rotor are quite sensible to the non linear terms of the hydrodynamic forces, it is applied the Newmark method with the convergence test being performed by the Newton-Rapshon method.

$$\begin{cases} \mu_{\boldsymbol{q}}(t) = \boldsymbol{q}_0, \\ \sigma_{\boldsymbol{q}}^2(t) = \langle\Phi_1^2\rangle\boldsymbol{q}_1^2 + \langle\Phi_2^2\rangle\boldsymbol{q}_2^2 + \langle\Phi_3^2\rangle\boldsymbol{q}_3^2 + \langle\Phi_4^2\rangle\boldsymbol{q}_4^2 + \langle\Phi_4^2\rangle\boldsymbol{q}_5^2. \end{cases} \tag{17}$$

5. RESULTS AND DISCUSSION

The statistics of the random solution in Eq. (17) are calculated for the rotor considering an implementation with Matlab®. In the analysis, it is compared the deterministic solution with the envelopes of the homogeneous PC and the Latin Hypercube (denoted as HCL), considering the uncertain parameters varying in the interval $[-20\%, 20\%]$. For constructing the envelopes, it was used 500 samples, since the methods could converge with this number of samples.

The samples were generated in the given variability interval considered for the the oil viscosity and the shaft's radius positioned at the bearings. In the particular, for the shaft's radius, because we are interested in the radial clearance, the variation is calculated with relation to the radial clearance parameter.

The values adopted for the rotor's parameters were the following: shaft's width of 0.780; shaft's diameter of 0.025 m; disc's diameter of 0.100 m; disc's thickness of 0.002 m; bearing's width of 0.001 m; bearing's diameter of 0.025 m; Young's modulus of 2.067 x 10^{11} Pa; material density of 7800 kg/m^3; Poisson's coefficient of 0.3; constant λ equal to zero; constant β equal to 2 x 10^{-4}; unbalanced load of 100 x 10^{-6} kg.m at 0º; rotation speed of 1500 RPM; radial clearance of 50 x 10^{-6} m; oil viscosity of 0.04 Pa.s; and, shaft's radius at the bearings of 0.0125 m.

The rotor's motion of equation was solved for the time t varying in the interval of $[0, 10]$ seconds. The initial conditions are set to zero for the displacements and velocities, considering the time $t = 0$, for all the degrees of freedom. For the Newmark method, the following parameters were adopted: $\gamma = 0.5$, $\beta = 0.25$, and step size $h = 0{,}001$. Besides that, the Newton-Rapshon method converged when the norm of the residual vector was below to 10^{-5}.

The results in Figs. 2 to 5 show the transversal displacements of the nodes where the bearings and discs are attached, in function of the time, as well as they present the orbits on the plane xz associated to these nodes. In all these figures, the left plots have the deterministic solution and the mean solution of the PC and HCL, while in the right plots there are the envelopes of the PC and HCL methods.

Observing the figures, we noticed the PC solution coincides with the deterministic one, while the HCL solution is somehow different of the deterministic one. Moreover, the solution envelopes of the HCL show some variability when compared with the deterministic solution (and this variability is more accentuated if observing the displacements at the bearings), while the envelopes of the PC present no variation with relation to the deterministic solution. Besides that:

- For the displacements associated with the bearing #1, Figs. 2b and 2d, we observe the upper and lower envelope lines of the HCL have a meaningful difference in the regions close to the peaks and valleys. This difference is better observed for the envelopes associated with the orbits in Fig. 2f.
- With relation to disc #1, the envelopes calculated with the HCL show the upper and lower lines are not close each other, although such difference are not clear in Figs. 3b and 3d, but instead, they can be noticed in the orbits in Fig. 3f. On the other hand, the envelopes of the PC present no difference between the upper and lower lines.
- The displacements related to the disc #2 are smaller than those ones of the disc #1. We can also notice the orbits of the disc #2, in Fig. 4f, have a smaller amplitude than those of disc #1, in Fig. 3f. Besides that, in Figs. 4b and 4d, the upper and lower lines of the envelope obtained with the HCL are distant from the deterministic solution, while the envelopes of the PC have their upper and lower lines coinciding with the deterministic solution.
- For the bearing #2, we notice its displacements present the same behavior of those of the bearing #1. With relation to the envelopes of the HCL, we observe that there is a difference between their upper and lower lines over all the orbit, in Fig. 5f, as well as for the transversal displacements, in Figs. 5b and 5d. Notice that the orbit of the bearing #2 has its amplitude bigger than that one of the bearing #1.

It is important to mention that the scale of values associated with the displacements in the bearings is smaller than the one in the discs, although the differences between the upper and lower lines of the envelopes are more perceptible in the figures with the bearings. This behavior is expected because each disc has an unbalanced mass, contrary to the bearings in which the displacements are limited to the radial clearance. We noticed the envelopes of the PC presented no variation between the upper and lower lines. The latter happened because the system in Eq. (16) is not coupled, then the coefficient $\boldsymbol{q}_0$, which is used to obtain the mean solution of the PC, can be computed by solving directly the first equation of such system. Note that such equation is not affected by the parameters σ_μ and σ_R, so there is no variability in the PC solutions.

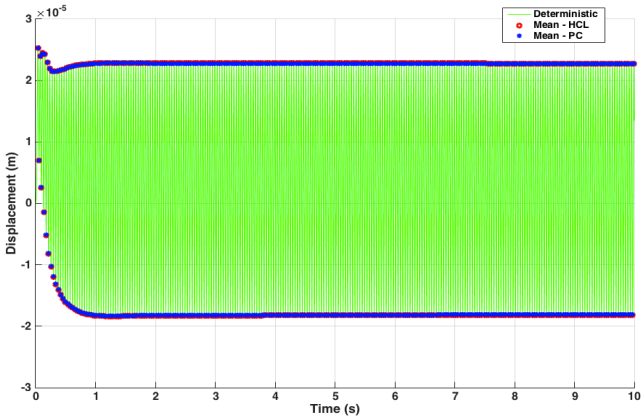

(a) Displacement on the direction of the x axis.

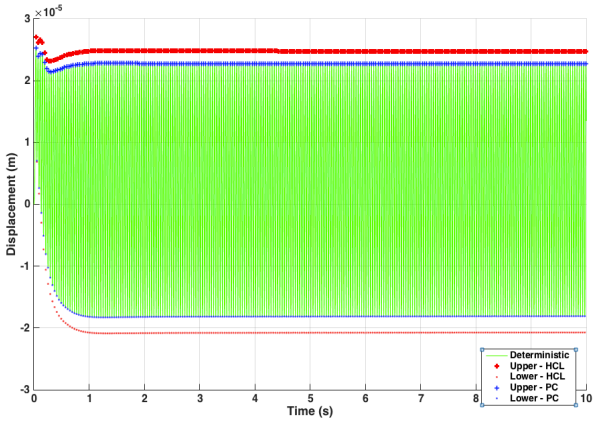

(b) Envelopes for the displacement on the x axis.

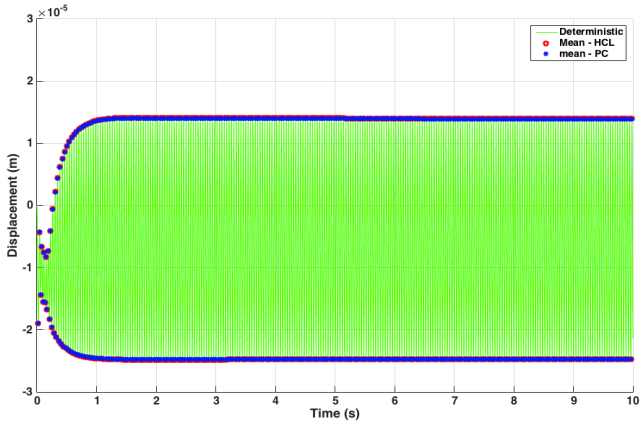

(c) Displacement on the direction of the z axis.

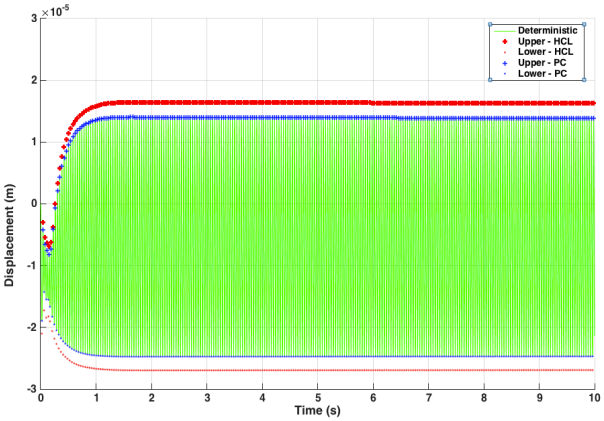

(d) Envelopes for the displacement on the z axis.

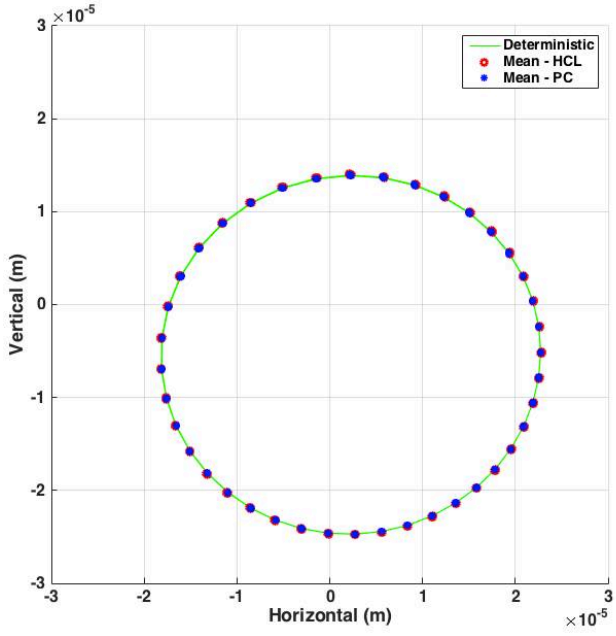

(e) Orbit.

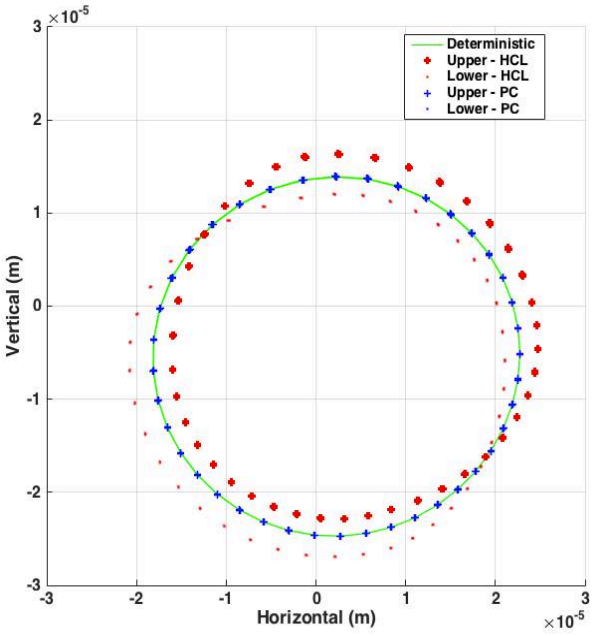

(f) Envelope of the orbits.

Figure 2. Transversal displacements and orbits of the bearing #1.

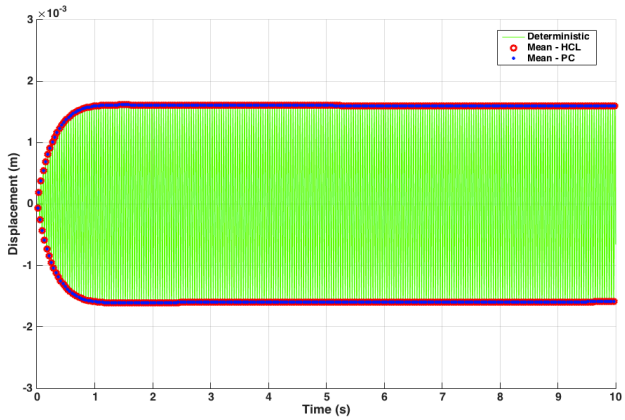

(a) Displacement on the direction of the x axis.

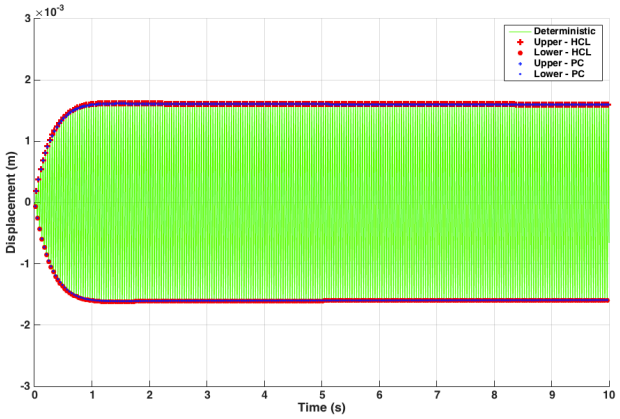

(b) Envelopes for the displacement on the x axis.

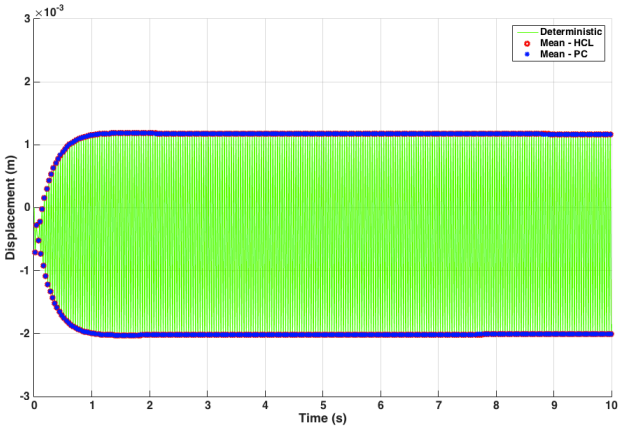

(c) Displacement on the direction of the z axis.

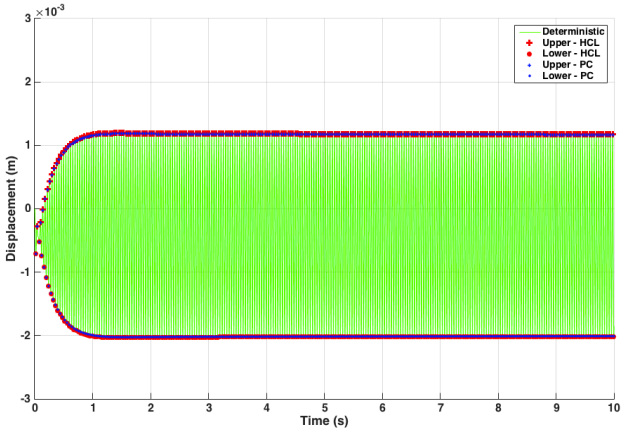

(d) Envelopes for the displacement on the z axis.

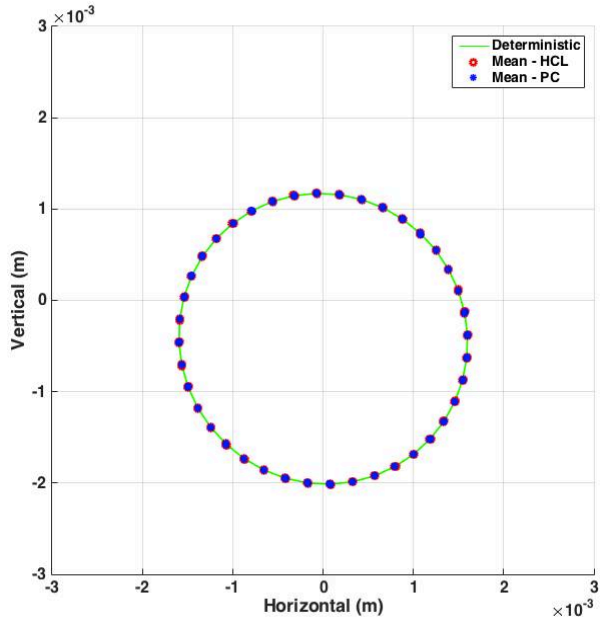

(e) Orbits.

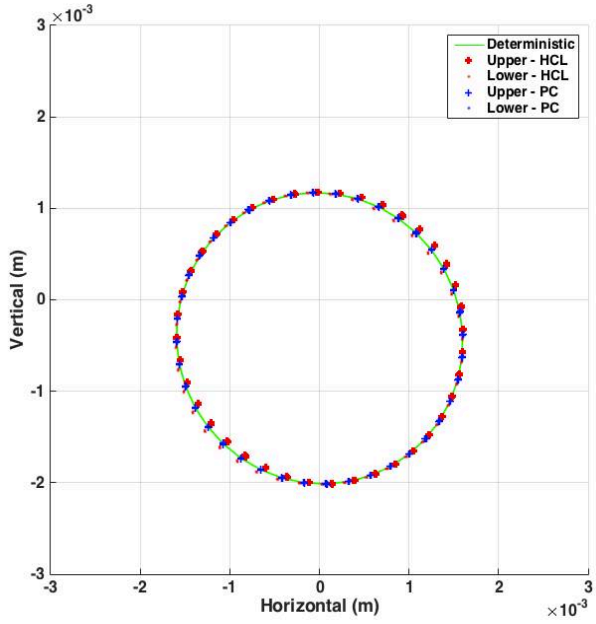

(f) Envelope for the orbits.

Figure 3. Transversal displacements and orbits of the disc #1.

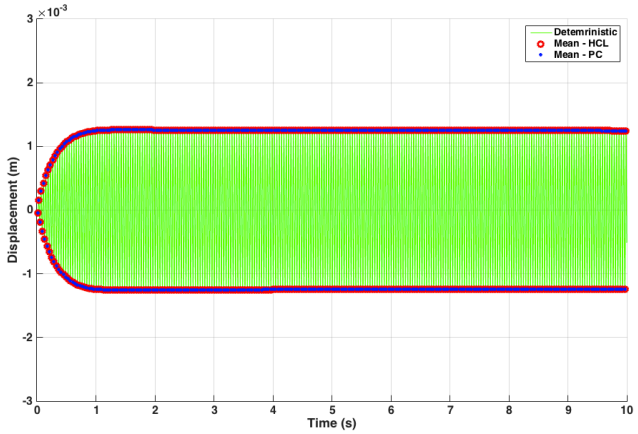

(a) Displacement on the direction of the x axis.

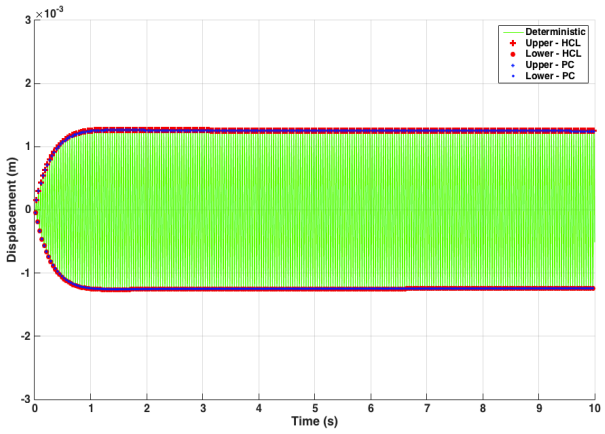

(b) Envelopes for the displacement on the x axis.

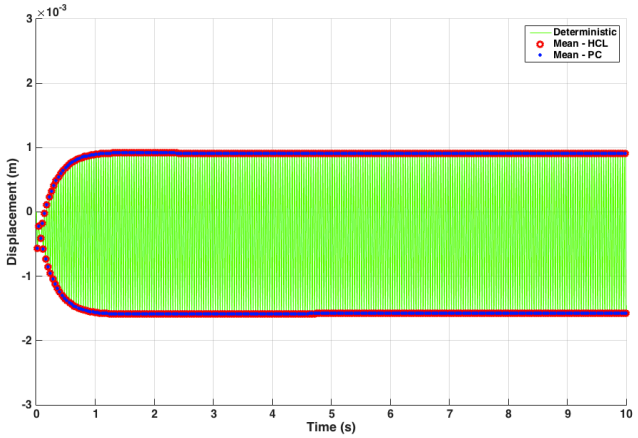

(c) Displacement on the direction of the z axis.

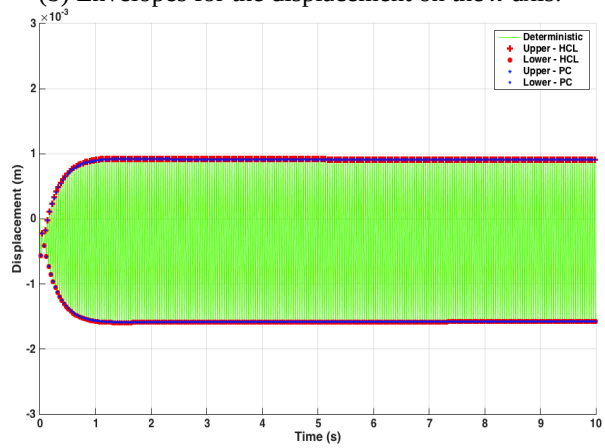

(d) Envelopes for the displacement on the z axis.

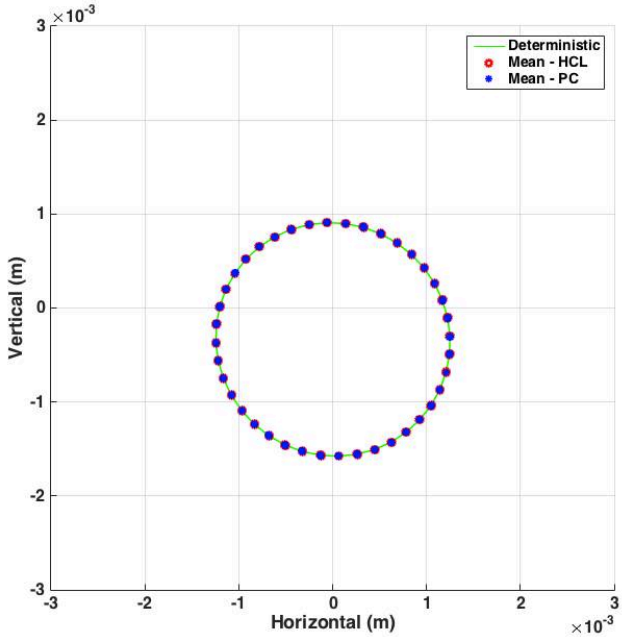

(e) Orbits.

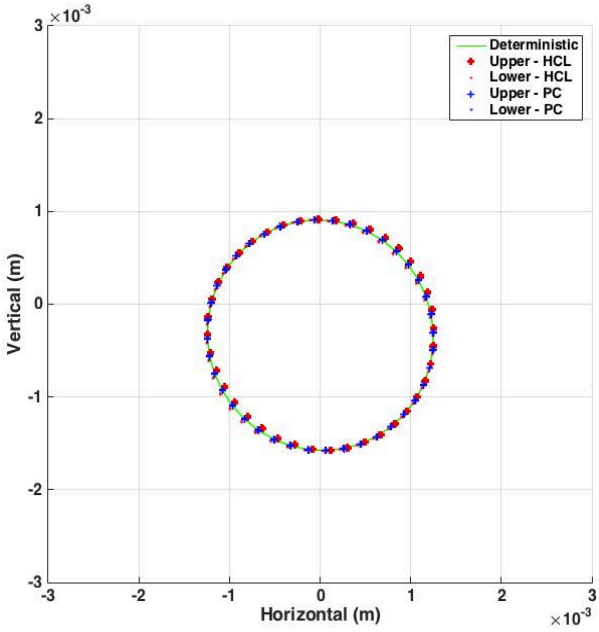

(f) Envelope for the orbits.

Figure 4. Transversal displacements and orbits of the disc #2.

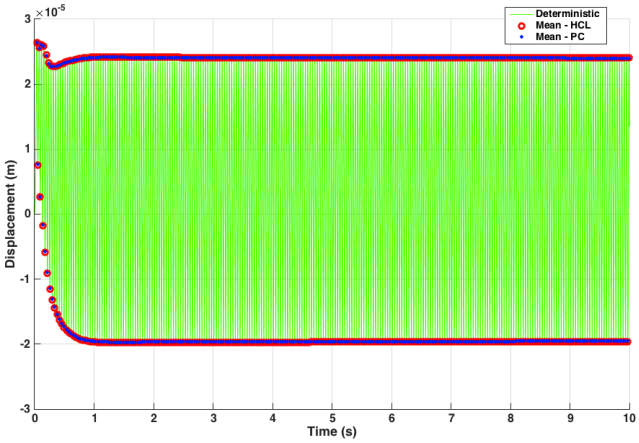

(a) Displacement on the direction of the x.

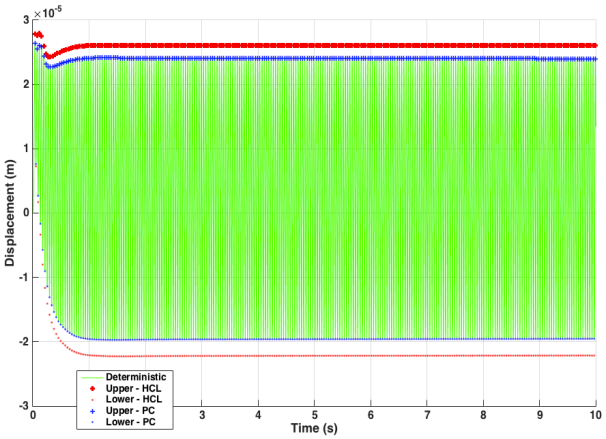

(b) Envelopes for the displacement on the x axis.

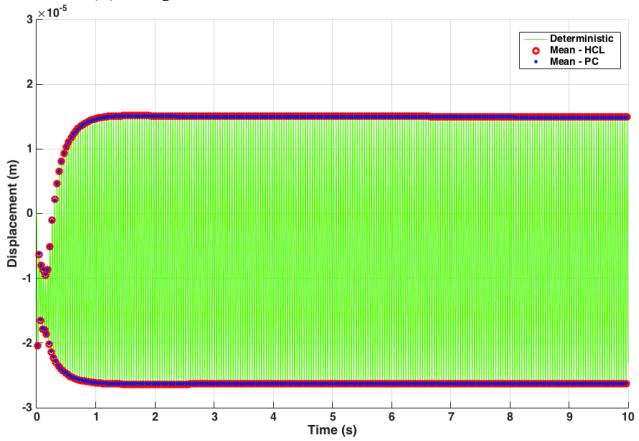

(c) Displacement on the direction of the z.

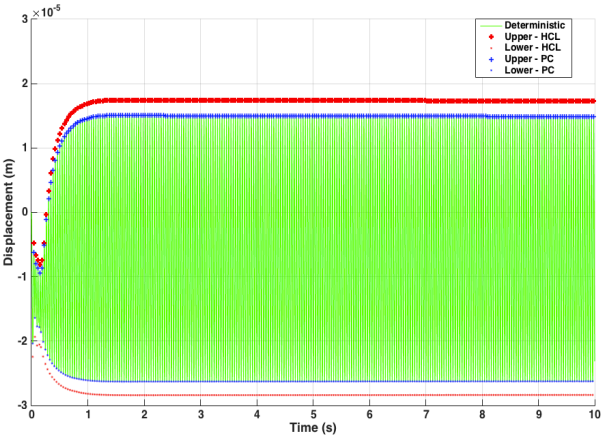

(d) Envelopes for the displacement on the z axis.

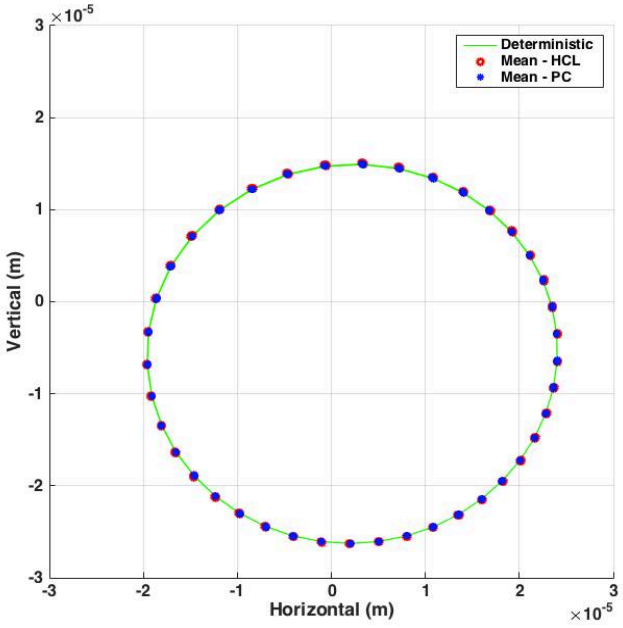

(e) Orbits.

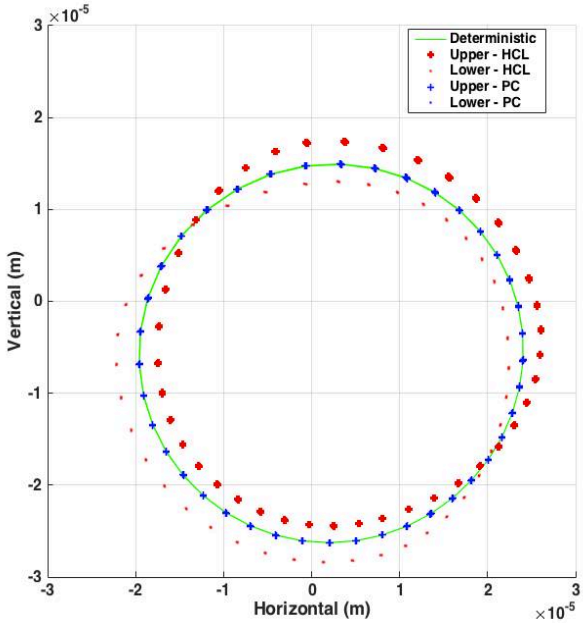

(f) Envelope for the orbits.

Figure 5. Transversal displacements and orbits of the bearing #2.

6. CONCLUSIONS

Aiming to handle with uncertainties in mechanical systems, this work considered the homogeneous polynomial chaos expansion applied on a flexible rotor in which the uncertainties were in the bearings. In the analysis, the oil viscosity and

the shaft's radius were considered as uncertain parameters. The solutions reported the displacements of the discs and bearings, as well as their orbits.

The numerical experiments for a flexible rotor with constant speed have shown that the PC's mean solutions and the deterministic ones are similar, while there is some variability when comparing the Latin Hypercube solutions and the deterministic ones. The solution envelopes computed with Latin Hypercube show that there is satisfactory variability in the transversal displacements of the discs because they can be influenced by an unbalanced mass, while the bearings limit the shaft movement. Analyzing the envelopes, it has been observed that the polynomial chaos is better than the Latin Hypercube, showing that the latter can require a considerable number of samples in order to obtain precise solutions.

Future works will consider new types of uncertainties in the rotor, for example, in the unbalanced forces, in the mass matrix and in the stiffness matrix as well. It is also desired to analyze the rotor in the run-down condition for the presence of uncertain parameters.

7. ACKNOWLEDGEMENTS

The authors are thankful to the Brazilian research agencies CNPq, FAPEG, and also to CAPES for the financial support provided to this research effort.

8. REFERENCES

Cai, D. and Xiao, H., 2016. "Dynamic Modeling and Analysis of Sliding Bearing-Rotor System with Coupling Rubbing Faults". In *Proceedings of the 2016 Sixth International Conference on Instrumentation & Measurement, Computer, Communication and Control (IMCCC)*, Harbin, China, p. 163-166.

Capone, G., 1986. "Orbital motions of rigid symmetric rotor supported on journal bearings". *La Meccanica Italiana*, n. 199, p. 37-46.

Cavalini Jr, A.A., Lara-molina, F.A., Sales, T.P., Koroishi, E.H. and Steffen Jr, V., 2015. "Uncertainty analysis of a flexible rotor supported by fluid film bearings". *Latin American Journal of Solids and Structures*, Vol. 12, n. 8, p. 1487-1504.

Daróczy, D., Janiga, G. and Thévenin, D., 2016. "Analysis of the performance of a H-Darrieus rotor under uncertainty using Polynomial Chaos Expansion". *Energy*, Vol. 113, p. 399-412.

Ghanem, R. G.; Spanos, P. D., 1991. *Stochastic Finite Elements: a Spectral Approach.* Springer-Verlag.

Lalanne, M. and Ferraris, G., 1998. *Rotordynamics prediction in engineering*. John Wiley and Sons, New York, 2nd edition.

Lucor, D., Su, C.-H. and Karniadakis, G.E., 2004. "Generalized polynomial chaos and random oscillators". *International Journal for Numerical Methods in Engineering*, Vol. 60, p. 571-596.

Machado, T.H. and Cavalca, K.L., 2015. "Modeling of hydrodynamic bearing wear in rotor-bearing systems". *Mechanics Research Communications*, Vol. 69, p. 15-23.

Mendes, R.U., Machado, T.H. and Cavalca, K.L., 2017. "Experimental wear parameters identification in hydrodynamic bearings via model based methodology". *Wear*, Vol. 372-373, p. 116-129.

Muszynka, A.A., 2005. *Rotordynamics*. CRC Press.

Sinou, J.-J. and Jacquelin, E., 2015. "Influence of Polynomial Chaos expansion order on an uncertain asymmetric rotor system response". *Mechanical Systems and Signal Processing*, Vol. 50-51, p. 718-731.

Viana, F.A.C., 2016. "A Tutorial on Latin Hypercube Design of Experiments". *Quality and Reliability Engineering International*, Vol. 32, n. 5, p. 1975-1985.

Xiu, D., Lucor, D., Su, C.-H. and Karniadakis, G.E., 2003. "Performance Evaluation of Generalized Polynomial Chaos". In *Proceedings of the International Conference on Computational Science (ICCS 2003)*, p. 346-354.

Xiu, D. and Karniadakis, G.E., 2002. "The Wiener-Askey polynomial chaos for stochastic differential equations". *SIAM Journal on Scientific Computing*, Vol. 24, n. 2, p. 619-644.

9. RESPONSIBILITY NOTICE

The authors are the only responsible for the printed material included in this paper.